Journal of Cerebral Blood Flow & Metabolism (2015) 35, 676–683

www.jcbfm.com

ORIGINAL ARTICLE

The spectrum of MR detectable cortical microinfarcts: a classification study with 7-tesla postmortem MRI and histopathology

Susanne J van Veluw[1], Jaco JM Zwanenburg[2], Annemieke JM Rozemuller[3], Peter R Luijten[2], Wim GM Spliet[3] and Geert Jan Biessels[1]

Cerebral microinfarcts (CMIs) are common neuropathologic findings in aging and dementia. We explored the spectrum of cortical CMIs that can be visualized with 7T magnetic resonance imaging (MRI). Thirty-three coronal brain slices of 11 individuals with neuropathologically confirmed dementia were subjected to a high-resolution postmortem 7T MRI protocol. First, we identified all visible small (⩽5 mm) intracortical and juxtacortical lesions on postmortem MRI. Lesions were classified as CMI or nonCMI based on histology, and their MR features were recorded. Thirty lesions were identified on the initial MRI evaluation, of which twenty-three could be matched with histology. Histopathology classified 12 lesions as CMIs, all of which were located intracortically. On the basis of their MR features, they could be classified as chronic gliotic CMIs—with or without cavitation or hemorrhagic components—and acute CMIs. Eleven MRI identified lesions were not of ischemic nature and most commonly enlarged or atypically shaped perivascular spaces. Their MRI features were similar to gliotic CMIs with or without cavitation, but these 'CMI mimics' were always located juxtacortically. 7T postmortem MRI distinguishes different histopathologic types of cortical CMIs, with distinctive MR characteristics. On the basis of our findings, we propose *in vivo* rating criteria for the detection of intracortical CMIs.

Journal of Cerebral Blood Flow & Metabolism (2015) **35,** 676–683; doi:10.1038/jcbfm.2014.258; published online 21 January 2015

Keywords: 7-tesla MRI; dementia; histopathology; microinfarcts; postmortem; small vessel disease

INTRODUCTION

Cerebral microinfarcts (CMIs) are common neuropathologic findings in the aging human brain.[1,2] They are manifestations of small vessel disease and show a strong association with antemortem cognitive decline and dementia.[3,4] A systematic review of autopsy studies reported frequencies of 43% in patients with Alzheimer's disease, 62% in patients with vascular dementia, and 24% in nondemented older individuals.[2] Due to their widespread and numerous appearance, they are increasingly recognized as substantial contributors to aging-related cognitive decline and dementia. Cerebral microinfarcts are hardly visible on gross pathology, but on routine pathologic examination of microscopic sections they can be identified as small delineated regions of tissue pallor. They are characterized by neuronal death and gliosis, and sometimes they are accompanied by cavitation or macrophages, that may contain hemosiderin. Their reported sizes vary between 50 μm and a few mm, making them hard to detect *in vivo* with conventional magnetic resonance imaging (MRI).

Recently, we have shown that cortical CMIs can be visualized *in vivo* with high-field 7-tesla MRI.[5] In that study, we developed an operational MRI definition for these lesions that proved to be specific for cortical CMIs on postmortem MRI guided histopathologic examination. According to that definition, cortical CMIs are intracortical lesions, hyperintense on fluid-attenuated inversion recovery (FLAIR) and on T2, hypointense on T1, ⩽3 mm in size, and distinct from perivascular spaces (PVSs).[5] In this initial study, we purposefully devised a definition that was likely to be specific for CMIs, because our intention was to show feasibility of *in vivo* CMI detection. It could well be, however, that this definition misses certain cortical CMIs that are visible on MRI, but have different MRI characteristics. Therefore, the current study was designed to explore the whole spectrum of cortical CMIs that can be captured with 7-tesla MRI. First, we identified all MRI-visible small (⩽5 mm) intracortical as well as juxtacortical lesions on postmortem MRI of human brain tissue. Only lesions that were obviously an artifact or regularly shaped PVSs were discarded. The MR features of these lesions were noted and their histopathologic substrate was verified. All lesions that proved to be CMIs were classified in different subtypes. All lesions that proved to be of nonischemic nature were also classified based on their histology and MRI appearance, to identify potential CMI mimics and their distinguishing features.

MATERIALS AND METHODS

Patients and Tissue

Brain specimens of patients who had undergone autopsy in the preceding 2 years at the University Medical Center Utrecht (UMCU) were included in

[1]Department of Neurology, Brain Center Rudolf Magnus, University Medical Center Utrecht, Utrecht, The Netherlands; [2]Department of Radiology, University Medical Center Utrecht, Utrecht, The Netherlands and [3]Department of Pathology, University Medical Center Utrecht, Utrecht, The Netherlands. Correspondence: SJ van Veluw, Department of Neurology G03.232, University Medical Center Utrecht, PO Box 85500, 3508 GA Utrecht, The Netherlands.
E-mail: s.j.veluw-2@umcutrecht.nl
This work was supported by a VIDI grant from ZonMw, The Netherlands Organization for Health Research and Development (91711384), and a clinical established investigator grant from the Netherlands Heart Foundation (2010 T073) to GJB. The research leading to these results is also based on support from the European Research Council under the European Union's Seventh Framework Program (FP7/2007-2013)/ERC grant agreement no 337333 to JZ.
Received 14 October 2014; revised 15 December 2014; accepted 17 December 2014; published online 21 January 2015

this study. After autopsy, the brains were fixated in 10% formalin before they were cut into 10-mm-thick coronal brain slices. Standard neuropathologic examination was performed to establish a diagnosis. Cases were selected from the database of the neuropathology department based on recorded presence of considerable Alzheimer pathology (Braak & Braak (BB) stage $\geqslant$ III), cerebral amyloid angiopathy (CAA), or vascular dementia (Supplementary Table 1). Hence, 11 cases were eligible for inclusion. From each case, three brain slices were selected for postmortem imaging. They were taken from the frontal, temporo-parietal, and occipital lobes (Supplementary Figure 1). For each scan session, three slices submerged in 10% formalin were placed in a purpose-built Perspex container that was designed to fit in the head coil of the MR scanner. Care was taken to avoid air bubbles. The use of the brain specimens of these patients for this study was in accordance with local regulations and approved by the medical ethics committee of the UMCU. Informed consent was obtained before autopsy, according to local (UMCU) ethical guidelines.

Study Design

In total, 33 brain slices were scanned and evaluated for intracortical and juxtacortical lesions. All identified lesions were sampled and subjected to histopathologic examination. Finally, we also explored areas in which no lesions were identified on MRI. These 'MR negative control areas' were sampled, subjected to histopathologic examination, and screened for CMIs histopathologically. More details are provided below.

Postmortem Magnetic Resonance Imaging Protocol

Scans were acquired overnight on a whole-body 7-tesla MR system (Philips Healthcare, Cleveland, OH, USA) with a volume transmit and 32-channel receive head coil (Nova Medical, Wilmington, MA, USA). The specimen remained embedded in formalin during scanning. The protocol, optimized for postmortem imaging, included the following sequences:

1. 3D FLAIR with an acquired isotropic resolution of $400 \times 400 \times 400\ \mu m^3$, repetition time (TR) = 8,000 ms, nominal echo time (TE) = 164 ms using constant low refocusing angles of 40°, inversion time (TI) = 1,600 ms (for nulling the formalin surrounding the tissue), matrix size = 500×280, 100 slices, no sensitivity encoding (SENSE) acceleration was applied. Scan duration 4 hours 16 minutes 8 seconds.
2. 3D T2-weighted turbo spin echo (TSE) with an acquired isotropic resolution of $400 \times 400 \times 400\ \mu m^3$, TR = 3,500 ms, nominal TE = 164 ms using constant low refocusing angles of 40°, matrix size = 500×280, 100 slices, no SENSE acceleration was applied. Scan duration 1 hour 52 minutes 3 seconds.
3. 3D T1-weighted sequence with an acquired isotropic resolution of $400 \times 400 \times 400\ \mu m^3$, TR = 7.7 ms, TE = 3.5 ms, post-inversion delay 280 ms, TR between inversion pulses 2,000 ms, matrix size = 348×348, 80 slices, no SENSE acceleration was applied. Scan duration 55 minutes 38 seconds.
4. 3D T2*-weighted sequence with an acquired isotropic resolution of $180 \times 180 \times 180\ \mu m^3$, flip angle 25°, TR = 75 ms, TE = 20 ms, matrix size = 832×834, 278 slices, no SENSE acceleration was applied. Scan duration 4 hours 59 minutes 31 seconds.

Magnetic Resonance Imaging Rating and Sampling

The acquired postmortem FLAIR and T2 MRI scans were screened for intracortical and juxtacortical (i.e., adjacent to and in direct contact with the cortex) small lesions $\leqslant$ 5 mm by an experienced rater. To ensure that the whole spectrum of MRI detectable CMIs was captured, we did not limit sampling to lesions with prespecified MRI features regarding signal intensity or shape. In other words, we did not limit sampling to lesions with imaging features considered to be typical for ischemic lesions. Hence, hypointense lesions possibly reflecting cortical microbleeds were also sampled. Regularly shaped extensions from a PVS, or evident postmortem tissue damage were not considered for sampling. Widely enlarged or otherwise atypically shaped PVSs in direct contact with the cortex was sampled. A juxtacortical PVS was regarded widely enlarged, if it stood out from the other PVSs in the same tissue, or if the signal intensity matched that of a possible cavitated ischemic lesion. The location of the lesions within the cortex, size (as measured on T2 in the greatest dimension of the lesion), and appearance on all MRI sequences were noted. To obtain accurate histologic sampling, the sampling was guided by the estimated depth of the lesion from the slice thickness of the MR images, and tissue architecture.

Cortical areas without lesions on MRI were also sampled, to identify additional CMIs that might have been missed by initial visual inspection of the MR images. Eleven samples were taken from the cortex (1 sample per case), at locations where no lesions were seen on MRI, preferably in a brain slice where no other samples were taken (Supplementary Figure 1). These comprised the 'MR negative control samples' (measuring approximately $30 \times 20 \times 5$ mm).

Histology and Immunohistochemistry

All samples were dehydrated, embedded in paraffin, and cut into 4-μm-thick sections. Standard Hematoxylin & Eosin (HE) and Luxol Fast Blue–Periodic Acid Schiff (LP) staining was performed on the first two adjacent sections. All HE and LP sections were examined by an experienced neuropathologist, blinded to the postmortem MR images. Next, histologic sections were compared with the MR images. In case the MR identified lesion was not found on the first section, three additional serial 4-μm-thick sections with a slice gap of 500 μm were cut. At each level, the first two adjacent sections were stained with HE and LP. When a CMI was identified, standardized immunohistochemistry (CD68, glial fibrillary acidic protein (GFAP), and β Amyloid) and histochemistry (Iron) was performed on adjacent sections. Lesion characteristics such as size (as measured on the HE section in the greatest dimension of the CMI), the presence of ischemic neurons, gliosis, cavitation, or hemosiderin-containing macrophages were noted.

RESULTS

Patient and brain tissue characteristics and results are provided in Supplementary Table 1. The patients had a mean age at death of 77.9 years (SD 7.9), 3 were men. One patient had a pathologic diagnosis of vascular dementia and three patients had Alzheimer pathology (BB $\geqslant$ IV). The other patients had mixed pathologies; three patients Alzheimer pathology (BB $\geqslant$ II) with CAA, two patients Alzheimer pathology (BB $\geqslant$ IV) with Lewy bodies, one patient Alzheimer pathology (BB II/III) with hypoxic-ischemic damage, and one patient Alzheimer pathology (BB IV) with both CAA and Lewy bodies. In total, 33 brain slices dissected from 11 whole brains were subjected to postmortem MRI. On the obtained MR images, 30 lesions were marked. Eighteen were located intracortically and 12 juxtacortically.

Intracortical Lesions

In all, 13 out of 18 intracortical lesions could be matched on the corresponding histologic sections, of which 12 proved to be a CMI. These CMIs could be classified into different types, based on their MRI features. These types include chronic gliotic CMIs—with or without cavitation or hemorrhagic components—and acute CMIs.

Chronic CMIs. Chronic gliotic CMIs were always hyperintense on T2-weighted and FLAIR images (Figure 1). On T1 they were generally hypointense. On MRI their mean size was 2.4 ± 0.5 mm ($n = 5$). Upon histopathologic examination, these gliotic CMIs appeared as demarcated regions of tissue pallor, accompanied by neuronal loss and gliosis. Sometimes a vessel could be discerned in the core of the gliotic CMI. On histology the mean size of these five CMIs was 1.7 ± 0.6 mm.

Chronic gliotic CMIs with cavitation were hyperintense on T2, and hypointense with a hyperintense rim on FLAIR (Figure 2). On T1 they appeared isointense with the surrounding fluid. On MRI their mean size was 3.0 ± 0.8 mm ($n = 3$). These CMIs were gliotic CMIs with an old, fluid-filled cavity on the histological and adjacent immunohistochemical sections. On histology their mean size was 1.3 ± 0.4 mm ($n = 3$).

Chronic gliotic CMIs with hemorrhagic components always appeared hypointense on T2-, FLAIR, and T2*-weighted images

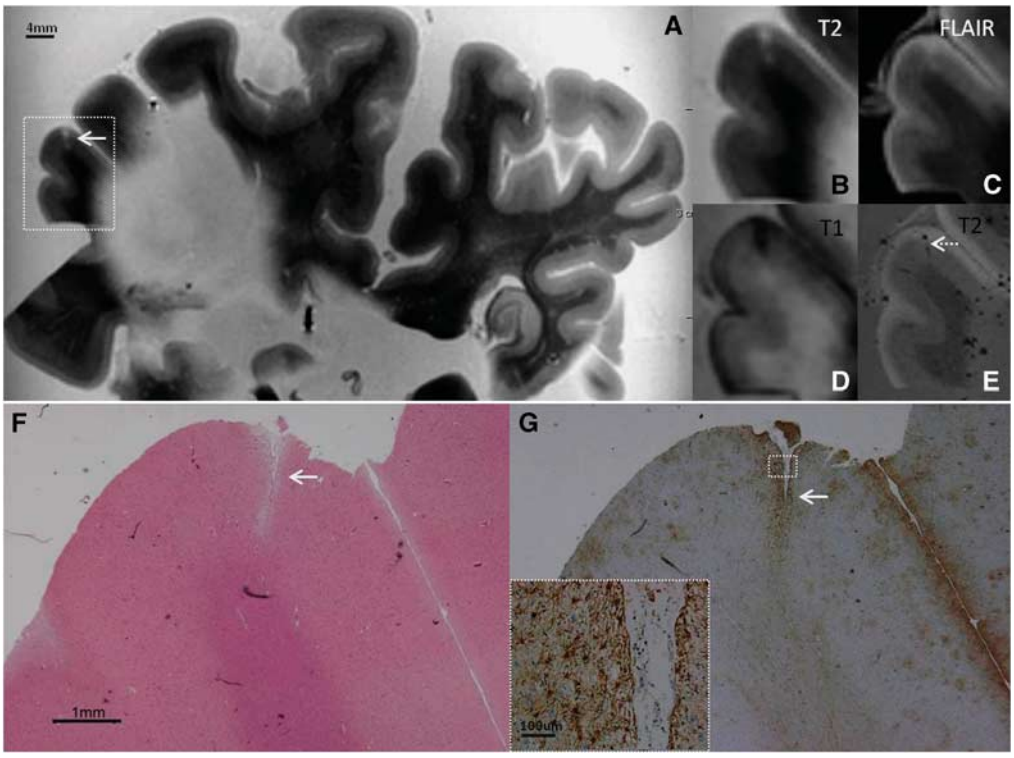

Figure 1. Intracortical chronic gliotic noncavitated microinfarct (indicated by arrow), identified on magnetic resonance imaging (MRI), in postmortem brain of a 78-year-old female with mild Alzheimer pathology (Braak & Braak (BB) II) and cerebral amyloid angiopathy (CAA). The intracortical gliotic microinfarct appeared hyperintense on T2 (**A**, enlarged in **B**) and FLAIR (**C**), and hypointense on T1 (**D**). On T2* a vessel (possibly filled with air or clotted blood) could be seen at the same location (**E**; broken arrow). On Hematoxylin & Eosin (HE) the microinfarct was identified as a region of tissue pallor, accompanied by neuronal death and gliosis (**F**). The adjacent section was GFAP positive, indicating the presence of astrogliosis (**G**; inset is enlargement of area indicated with white square). FLAIR, fluid-attenuated inversion recovery; GFAP, glial fibrillary acidic protein.

(Figure 3). On MRI their mean size was 2.3 ± 0.6 mm ($n = 3$). The same hemorrhagic CMIs were seen, on histopathologic examination, as focal accumulations of hemosiderin-containing macrophages, accompanied by gliosis and neuronal loss. The adjacent sections were positive for iron. On histology their mean size was 1.2 ± 0.7 mm ($n = 3$).

Acute CMIs. One CMI was slightly hypointense—isointense with the adjacent white matter—with a subtle surrounding hyperintense rim on both T2 and FLAIR (Figure 4). On MRI this CMI measured 4.0 mm ($n = 1$). The same CMI was identified upon histopathologic examination as a delineated area containing red neurons, but without astrocytes and macrophages, indicating it was an acute (< 24 hours) ischemic lesion. The area was demarcated by a region of tissue pallor. This acute CMI measured 4.4 mm on histology.

On MRI CMIs were located in all cortical layers, usually comprising multiple layers. Several CMIs however were typically restricted to the upper cortical layers, causing a localized dip (i.e., focal thinning) of the cortical surface.

It should be noted that some chronic gliotic CMIs were accompanied by incomplete cavitation on histology, not large enough to yield the characteristic hypointense signal with a surrounding hyperintense rim on FLAIR.

One intracortical MR identified lesion proved to be tissue rarefaction upon histopathologic examination (i.e., altered staining density of unknown nature). This 'lesion' had different MR characteristics than the CMI subtypes described above. It was rather inconspicuous on MRI, irregularly shaped, and had a patchy appearance (both in shape and in signal intensity), and hence could be distinguished from CMIs.

The MR features (i.e., location, size, and signal intensities) of the five intracortical lesions that could not be retrieved on histology were not clearly different from the lesions that were retrieved. Failure to retrieve these lesions was probably due to sampling errors, which can occur due to the small size of CMIs.

Juxtacortical Lesions

Ten out of 12 juxtacortical lesions could be matched on the corresponding histologic sections. None of these lesions proved to be a CMI on histologic examination.

Two lesions were hypointense on T2*, of which one was identified on histology as a primary hemorrhage, and one as a venous angioma. Their MR features were distinctive from the above described intracortical CMI subtypes. The primary hemorrhage was not well circumscribed or round with some penetration into the cortex. The venous angioma appeared as a cluster of tubular-shaped structures, hypointense on T2*.

Eight lesions proved to be PVSs. The PVSs had similar MR signal intensities as chronic gliotic CMIs with or without cavitation (Figure 5). Four appeared as small round lesions, located on the gray/white matter border, and were not readily identified as PVS based on their MR features alone. The other four had a tubular shape, were located perpendicular to the cortex, and appeared widely enlarged on MRI. Although the PVSs had similar MR signal intensities as chronic gliotic CMIs with or without cavitation, they could be discerned from the intracortical CMIs identified in this study either based on their shape (tubular) and location (juxtacortical), or just their location (gray/white matter border).

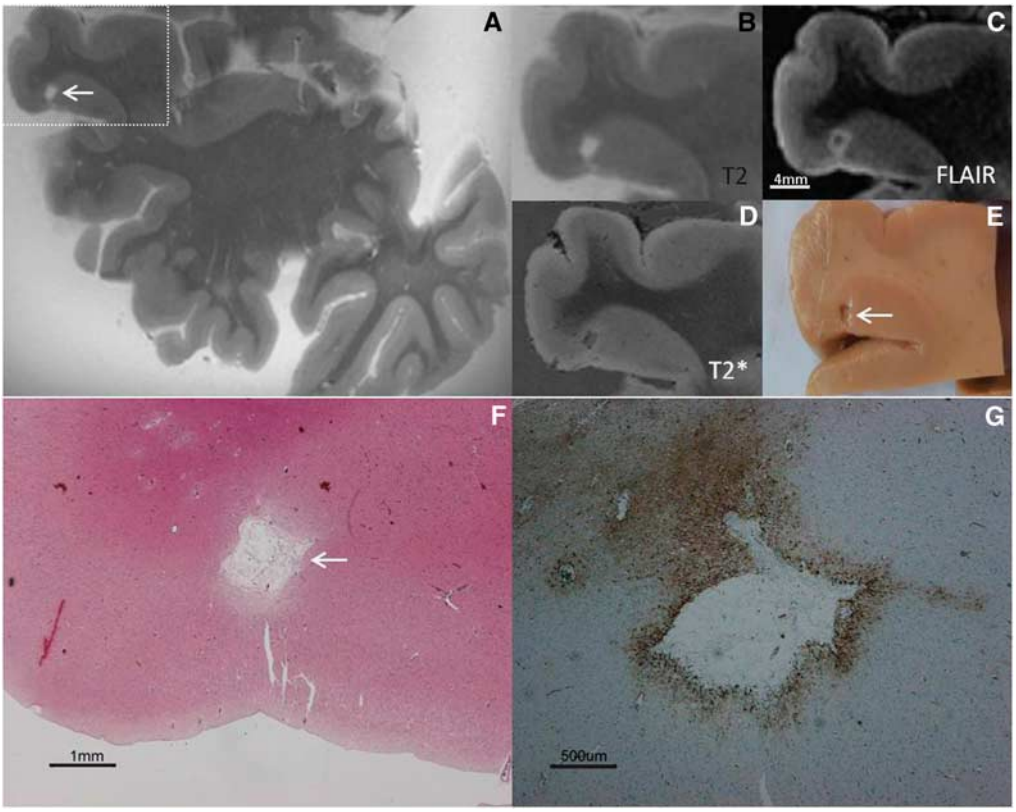

Figure 2. Intracortical chronic gliotic microinfarct with cavitation (indicated by arrow), identified on magnetic resonance imaging (MRI), in postmortem brain of an 86-year-old female with moderate Alzheimer pathology (Braak & Braak (BB) IV). The intracortical gliotic microinfarct with cavitation appeared hyperintense on T2 (**A**, enlarged in **B**), and hypointense surrounded by a hyperintense rim on FLAIR (**C**). On T2* the lesion was visible as a formalin filled cavity (**D**). This microinfarct was visible on gross pathology (**E**). On Hematoxylin & Eosin (HE) the microinfarct was identified as a region of tissue pallor, with neuronal death, gliosis, and accompanied by a cavity (**F**). The cavity was surrounded by a rim of gliosis, as indicated on the adjacent GFAP-positive section (**G**), corresponding to the hyperintense rim on FLAIR (**C**). FLAIR, fluid-attenuated inversion recovery; GFAP, glial fibrillary acidic protein.

The two juxtacortical lesions that could not be retrieved on histology appeared on MRI just like the other PVSs on the gray/white matter border.

Histopathologic Evaluation of Magnetic Resonance-Negative Control Samples

In the 11 MR-negative control samples that were taken from cortical areas without lesions on MRI, one intracortical CMI (size 1.0 mm) was identified upon microscopic examination of the histologic section. Upon re-evaluation of the MRI, this CMI could not be identified on T2, FLAIR, and T1, but could be matched with a hypointense alteration on T2*.

Twelve additional intracortical CMIs (mean size 0.6 ± 0.3 mm) were found in the MR-negative areas of ($n = 7$) samples that targeted MRI identified lesions. These CMIs were not identified on the initial MRI evaluation. All of these 12 intracortical CMIs were found in a single case (number 6), with severe CAA. None of these lesions could be identified with certainty upon re-evaluation of the corresponding MR images, but one could be matched with a hypointense lesion on T2* (Figure 3).

The 13 CMIs in the MR-negative areas were all characterized by tissue pallor on HE, and were accompanied by gliosis, and occasionally by cavitation or hemosiderin-containing macrophages.

Examples of Microinfarct Subtypes on *In Vivo* Magnetic Resonance Imaging

After completing the *ex vivo* experiments, we performed an exploratory survey to see whether the different CMI subtypes that were discernible on the postmortem MR images can also be found on *in vivo* 7 tesla MRI scans. We screened MR images of subjects with known cortical CMIs from previous 7-tesla studies.[5–8] These studies comprised MRI scans of subjects with early Alzheimer's disease, intracerebral hemorrhage, type 2 diabetes, and controls. Chronic gliotic CMIs with and without cavitation could be identified on *in vivo* 7-tesla MRI (Figure 6). However, chronic gliotic CMIs with hemorrhagic components could not be distinguished from cortical microbleeds. Both lesions seem to appear hypointense on T2-weighted images, and on T2*.

DISCUSSION

Postmortem MRI at 7 tesla is able to distinguish different histopathologic types of intracortical CMIs; chronic gliotic CMIs —with and without cavitation or hemorrhagic components—and acute CMIs. We did not observe CMIs in juxtacortical areas. Particularly in juxtacortical areas, PVSs can have MRI features that are very similar to those of CMIs.

All intracortical lesions that appeared hyperintense on T2 and FLAIR, and hypointense on T1, proved to be chronic gliotic CMIs on the retrieved histologic sections. This is in line with results from our previous MRI—histopathology study on 7-tesla MRI.[5] Apparently, these MRI features are specific for intracortical CMIs. When a chronic gliotic CMI is accompanied by cavitation or hemorrhagic components, this can be discerned on MRI. Chronic gliotic CMIs with cavitation were previously observed in a study that assessed cortical CMIs on *in vivo* 7-tesla MRI, in patients with spontaneous intracerebral hemorrhage.[6] Cerebral microinfarcts with cavitation are isointense with the surrounding fluid on T1. Because the brain

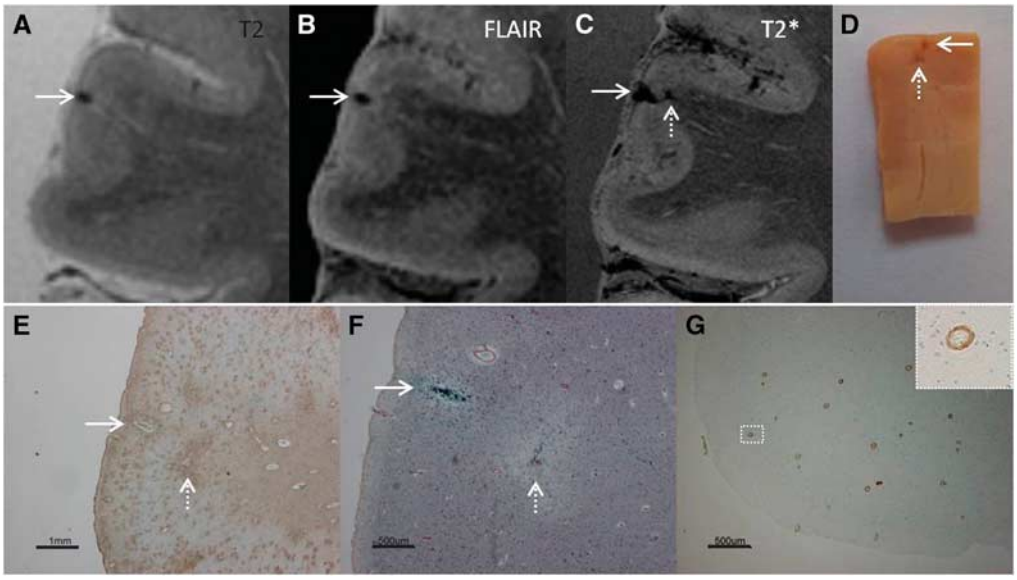

Figure 3. Intracortical chronic gliotic microinfarct with hemorrhagic components (indicated by arrow), identified on magnetic resonance imaging (MRI), in postmortem brain of a 78-year-old male with moderate Alzheimer pathology (Braak & Braak (BB) IV), Lewy body dementia (B V), and severe cerebral amyloid angiopathy (CAA). The intracortical gliotic microinfarct with hemorrhagic components appeared hypointense on T2 (**A**), FLAIR (**B**), and T2* (**C**) where it was enlarged due to the so-called 'blooming effect'. This microinfarct was already visible on gross pathology (**D**, arrow). On Hematoxylin & Eosin (HE) the microinfarct was identified as a region of tissue pallor, with neuronal death, gliosis, and accompanied by hemosiderin-containing macrophages (not shown here). The adjacent sections were positive for GFAP (**E**), CD68 (not depicted here), and iron (**F**). We did not observe any collapsed or ruptured vessels in the close proximity of the lesion. An additional microinfarct (indicated by broken arrow) was visible in the same section. This microinfarct was seen on gross pathology, but on MRI it could retrospectively only be matched to a hypointense lesion on T2* (broken arrow). This particular case showed severe CAA, as confirmed by Aβ immunohistochemistry (**G**; inset is enlargement from area indicated with white square). FLAIR, fluid-attenuated inversion recovery; GFAP, glial fibrillary acidic protein.

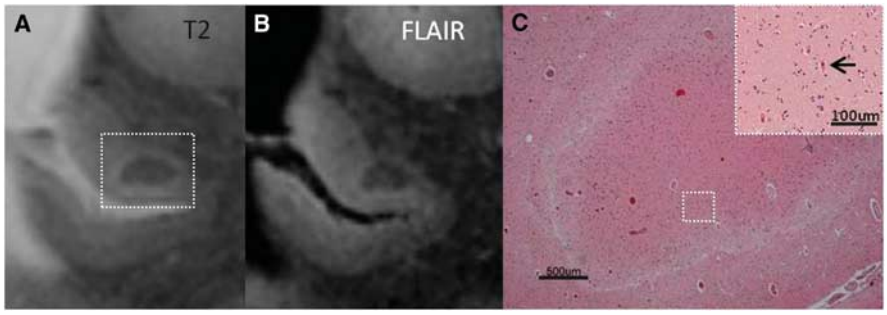

Figure 4. Intracortical acute microinfarct, identified on magnetic resonance imaging (MRI), in postmortem brain of a 76-year-old female with severe Alzheimer pathology (Braak & Braak (BB) IV/V). The microinfarct had the same signal intensity as the white matter on T2 (**A**) and FLAIR (**B**). On Hematoxylin & Eosin (HE) red neurons (indicative of acute neuronal injury) could be discerned in the area of infarction (**C**; arrow in inset). Furthermore, the adjacent sections were negative for both CD68 and GFAP (not depicted here), indicating that this microinfarct was approximately < 24 hours old. The white rim of tissue pallor surrounding the acute microinfarct corresponds to the subtle hyperintens rim on T2 and FLAIR (**A** and **B**). FLAIR, fluid-attenuated inversion recovery; GFAP, glial fibrillary acidic protein.

slices in the present postmortem study were scanned in formalin, gaining a high signal intensity of the fluid, CMIs with cavitation appeared hyperintense. On *in vivo* T1, cerebrospinal fluid is hypointense, resulting in a hypointense signal for cavitated CMIs on *in vivo* T1. Of note, cavitation can sometimes be very subtle, resulting in a hyperintense signal on FLAIR due to partial volume effects. This effect is probably larger on lower resolution images such as for *in vivo* 3-tesla MRI, implying that limited or partial cavitation is probably difficult to recognize on *in vivo* scans.

The MRI characteristics of CMIs with histopathologically confirmed hemorrhagic components, as described in this study overlap with the MRI characteristics of cerebral microbleeds (i.e., small areas of signal void with associated blooming seen on T2*-weighted MRI or other sequences that are sensitive to susceptibility effects[9]). Although the name 'microbleeds', puts emphasis on the 'hemorrhagic nature of these lesions', the few postmortem MRI studies that have examined the histopathologic correlates of MRI detected microbleeds report that the histopathology is heterogeneous (as reviewed by Shoamanesh *et al*[10]). Microbleeds were found to correlate with hemosiderin-containing macrophages (49%), old hemorrhages (16%), no specific pathology (15%), or intact erythrocytes (13%). One study[11] mentions that hemosiderin-containing macrophages in the basal ganglia were sometimes associated with minute areas of tissue necrosis. In another postmortem study of MRI detected microbleeds in the context of CAA,[12] some gliotic lesions with hemosiderin-laden macrophages were observed, which were interpreted as old, healed hemorrhage sites. However, it was noted that based on that study it could not be determined whether those lesions represent a primary ischemic pathology with secondary

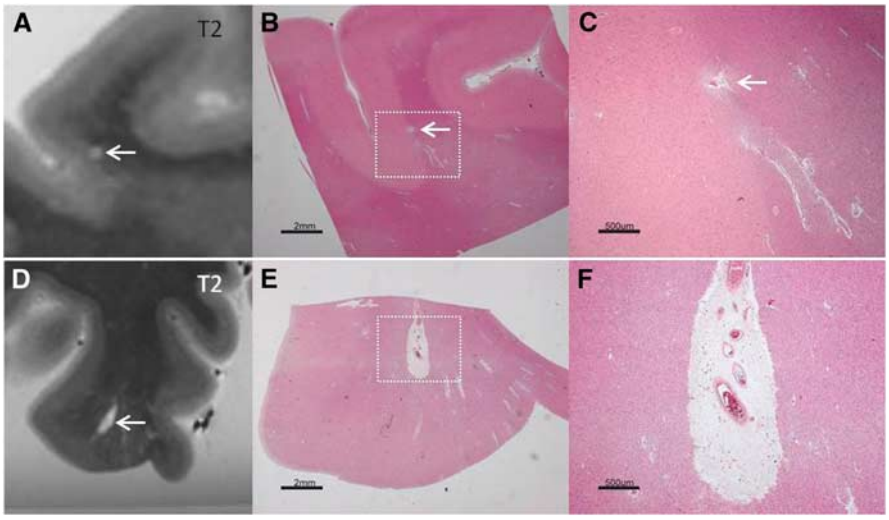

Figure 5. Two juxtacortical perivascular spaces (PVSs), identified on magnetic resonance imaging (MRI), in postmortem brain of a 78-year-old female with Alzheimer pathology (Braak & Braak (BB) II) and moderate cerebral amyloid angiopathy (CAA) (top row), and in postmortem brain of a 68-year-old female with Alzheimer pathology (BB VI) and severe CAA (bottom row). The first PVS was located on the gray/white matter border and had the same MRI features as chronic gliotic microinfarcts (**A**). On Hematoxylin & Eosin (HE) there was no evidence of neuronal death or gliosis (**B**, enlarged in **C**). The second enlarged-appearing tubular-shaped PVS was located perpendicular to the cortex and had the same MRI features as chronic gliotic microinfarcts with cavitation (**D**). On HE there was no evidence of neuronal death or gliosis (**E**, enlarged in **F**).

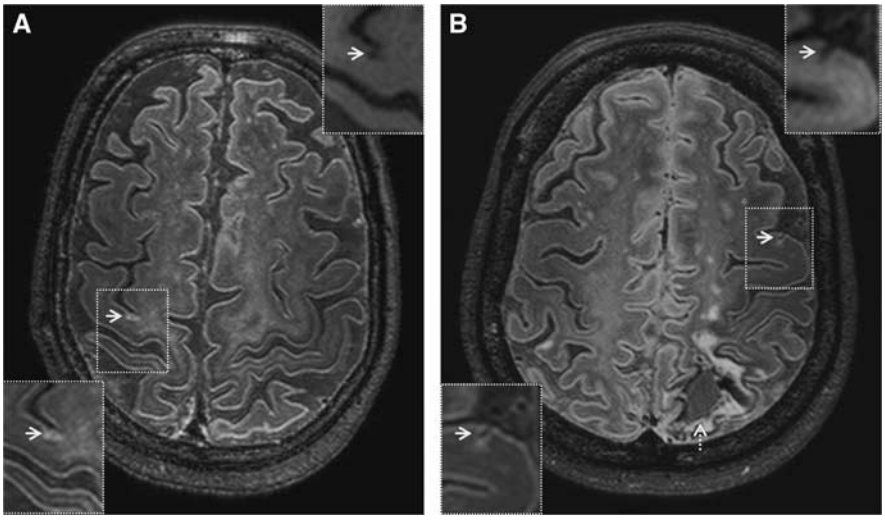

Figure 6. Cortical microinfarct subtypes on *in vivo* 7-tesla FLAIR (0.8 mm isotropic voxels) magnetic resonance imaging (MRI). A chronic gliotic microinfarct in a 76-year-old healthy male (**A**). A chronic gliotic microinfarct with cavitation in a 42-year-old female with spontaneous intracerebral lobar hemorrhage (indicated by broken arrow) (**B**; courtesy of Dr CJM Klijn, UMCU, The Netherlands). Insets in upper right corner are T1-weighted images (1.0 mm isotropic voxels). Chronic gliotic microinfarcts with and without cavitation are both hypointense on *in vivo* T1-weighted images. FLAIR, fluid-attenuated inversion recovery.

hemorrhage or tissue necrosis secondary to hemorrhage. The same holds true for the CMIs with hemosiderin-containing macrophages observed in our study. Further studies, both autopsy- and MRI-based, are needed to determine the exact histopathology of such lesions.

Likewise, MRI detected microbleeds can have different underlying etiology. It has been suggested that intracortical microbleeds on MRI are associated with CAA,[13,14] whereas MRI microbleeds in subcortical areas are related to hypertension.[15] In light of these observations, it remains currently not feasible to distinguish a chronic gliotic CMI with hemorrhagic components from a primary hemorrhage on MRI. More studies should look into the histopathologic correlates and underlying etiology of MRI identified 'microbleeds'. The same applies to the underlying etiology of CMIs. There is increasing evidence that CMIs are the result of severe CAA.[16–18] Other studies have suggested that CMIs may also be the result of hypoperfusion, or are caused by occlusions in small penetrating cortical vessels.[19] The latter may be due to abnormalities in the small vessels themselves or (micro)emboli. More studies are clearly needed to unravel the underlying etiology of CMIs, which seems to be heterogeneous.

Acute CMIs have previously been described on *in vivo* MRI as incident diffusion-weighted hyperintensities in the white matter.[1,20,21] It is known that hyperacute ischemic lesions can only appear on diffusion-weighted imaging and not on FLAIR. A multicenter study identified ischemic stroke patients within 4.5 hours of symptom onset based on a diffusion-weighted imaging —FLAIR mismatch with 62% sensitivity.[22] The acute CMI observed

Table 1. Proposed *in vivo* imaging criteria for cortical[a] microinfarcts in the context of aging and dementia

Type	T2	FLAIR	T1	T2*	DWI
1. Chronic					
a. Non-cavitated / non-hemorrhagic gliotic CMI, limited to the cortex, small (operationalized as ≤5 mm) (Fig. 6A)	Hyper	Hyper	Hypo	Iso	…
b. Cavitated / non-hemorrhagic gliotic CMI, limited to the cortex, small (operationalized as ≤5 mm) (Fig. 6B)	Hyper	Hypo + hyper rim	Hypo	Iso	…
c. Hemorrhagic gliotic CMI, limited to the cortex, small (operationalized as ≤5 mm)[#]	Hypo	Hypo	…	Hypo	…
2. Acute					
Non-gliotic CMI, limited to the cortex, small (operationalized as ≤5 mm)	Hypo (Iso with WM + hyper rim)	Hypo (Iso with WM + hyper rim)	…	…	Hyper[$]

Abbreviations: CMI, cerebral microinfarct; DWI, diffusion-weighted imaging; FLAIR, fluid-attenuated inversion recovery; MRI, magnetic resonance imaging. High-resolution 7-tesla 3D FLAIR, T2, and T1 currently offer the highest sensitivity and specificity for rating microinfarcts *in vivo*. Microinfarcts can also be detected on high quality 3D images at lower field strength (i.e., 3-tesla MRI), albeit with lower sensitivity than 7-tesla. *These criteria are only applicable for intracortical microinfarcts. Juxtacortical hyperintense lesions should best be discarded (see main text). … no data available yet. [$]Hemorrhagic gliotic CMIs can currently not be distinguished from primary microhemorrhages on MRI. Both will have the appearance of a 'microbleed' on MRI.

in our postmortem study was rather inconspicuous (i.e., not hyperintense) on FLAIR and would most likely escape detection on *in vivo* FLAIR. It would be interesting to follow acute CMIs over time, to see whether they change into chronic gliotic CMIs. Likewise it would be interesting to see whether chronic gliotic CMIs evolve into CMIs with cavitation longitudinally.

It is notable that we did not observe any lesions that proved to be CMIs in juxtacortical areas. Importantly, this observation is also corroborated by a re-evaluation of cases from pathologic studies (two community cohorts and one clinic cohort). On the basis of our observations, the exact locations of 80 CMIs in cortical areas from these cohorts were verified. None of these CMIs involved the white matter in juxtaposition to the cortex (personal communication, Julie Schneider, Rush University Medical Center, Chicago). The observation that juxtacortical areas appear to be spared from CMIs might be explained by the fact that the juxtacortical u-fibers receive blood supply from more than one source, namely the long penetrating medullary vessels and strictly cortical vessels. Also, the u-fibers are frequently spared in the case of widespread white-matter lesions.[23] Enlarged PVSs are a common finding in the white matter, especially in the context of CAA.[24] In our study, MR identified 'lesions' in juxtacortical areas that had similar appearance as intracortical CMIs proved to be PVSs on histology. When rating CMIs on *in vivo* MRI, juxtacortical hyperintense lesions should best be discarded.

The mean size of the CMIs on MRI was approximately 2 to 3 mm. Due to the small sample size, we were unable to compare lesion size between CMI subtypes. An interesting observation was that the size of CMIs was almost always larger on MRI than on the corresponding histologic section. This is likely due to a discordance in resolution. The voxel size of the T2 image is 0.4 mm^3, whereas the resolution of a microscopic section is much higher, allowing a more precise measurement of the size of a lesion. However, the 3D information in the MR image allows you to measure the lesion at its greatest dimension, whereas a 2D histology section is not always cut at the level of the greatest dimension of the lesion. Hence, a histologic section might underestimate the actual size of a CMI. This underlines the added value of postmortem (3D) MRI for the detection of CMIs. Other factors that might have a role in this discrepancy are the choice of MRI sequences, and the dehydration process before histopathologic preparation.

The majority of CMIs that were identified in the MR-negative histologic sections and proved to be invisible (i.e., too small) also on re-examination of the MRI, were observed in a single case, with severe CAA. Our findings suggest that only the larger CMIs (on average >2 mm) can be observed with high-resolution MRI. The CMIs that escaped detection were on average <1 mm. Extrapolating these findings to *in vivo* (i.e., lower resolution) MRI it is assumed that only the top of the iceberg of total CMI burden can be visualized. Estimates from neuropathological studies indicate that sizes of CMIs vary between 50 μm and 5 mm.[2] Hence, the CMIs that can be captured on MRI are likely to represent only a small fraction of the largest CMIs, probably with a much broader underlying lesion burden. However, this limitation is compensated by the fact that MRI allows whole brain coverage, while in autopsy studies typically only a small part of the brain is examined histopathologically. A recent study showed that observing one or a few CMIs on standard histopathologic examination is indicative for hundreds or even thousands of CMIs throughout the whole postmortem brain.[25] Probably, the observation of one or a few CMIs on *in vivo* MRI could indicate the presence of more smaller CMIs.

Our postmortem study supports and further refines previously applied criteria for the detection of CMIs on *in vivo* MRI.[7,8] On the basis of these findings, we propose *in vivo* rating criteria for intracortical CMIs and their subtypes (Table 1). Chronic gliotic CMIs are hyperintense on T2 and FLAIR, and hypointense on T1. Cavitated CMIs are hypointense on FLAIR with a hyperintense rim. Despite lower signal-to-noise ratio and resolution, it seems

feasible to recognize chronic gliotic CMIs on 3-tesla MRI as well.[5,26–28] Hemorrhagic CMIs cannot currently be distinguished from primary hemorrhages, both will be regarded as cerebral microbleeds on *in vivo* MRI. Juxtacortical hyperintense lesions should best be discarded.

The strength of this study is that we used high-resolution postmortem brain MRI, combined with a direct histopathologic validation of observed lesions. Moreover, these findings are translated to *in vivo* MRI, which warrants the study of different types of CMIs, possibly with a different underlying etiology, and their role in aging and dementia in living patients. The clinical relevance of the different CMI subtypes has to be determined in studies—both *in vivo* and *ex vivo*—involving larger patient samples.

This study has some limitations. First of all, the sample size is relatively small. Because long tissue storage influences MR quality,[29] only recent cases were selected. However, with high-resolution images of whole coronal sections, even a small sample size allowed us to study many lesions. Second, several possible CMIs could not be matched on the corresponding histologic sections, even after serial sectioning. Although we aimed for a precise localization of the CMIs, based on the detailed MR images, retrieving the corresponding CMIs on a histologic section proved to be challenging. This was probably due to the applied slice gap (of 500 μm) for serial sectioning. Ideally, one would cut the entire tissue block, but this would be very time consuming and costly. Of note, however, the MR features of the lesions that were missed on histology were not typically different from the lesions that could be retrieved.

CONCLUSIONS

In conclusion, postmortem MRI at 7-tesla distinguishes different histopathologic types of intracortical CMIs, with distinctive MRI characteristics. On the basis of our findings, we propose *in vivo* rating criteria for the detection of intracortical CMIs. Caution is warranted with rating CMIs in juxtacortical regions, as these regions may contain fewer CMIs, but do contain important CMI mimics, in particular PVSs.

DISCLOSURE/CONFLICT OF INTEREST

The authors declare no conflict of interest.

ACKNOWLEDGMENTS

The authors thank Julie Schneider and Chenhui Yang for providing additional pathological data on microinfarct location. Samples were reviewed from the Religious Orders Study, the Rush Memory and Aging project, and the Rush Alzheimer's disease center Clinical Core.

REFERENCES

1 Smith EE, Schneider JA, Wardlaw JM, Greenberg SM. Cerebral microinfarcts: the invisible lesion. *Lancet Neurol* 2012; **11**: 272–282.
2 Brundel M, de Bresser J, van Dillen JJ, Kappelle LJ, Biessels GJ. Cerebral microinfarcts: a systematic review of neuropathological studies. *J Cereb Blood Flow Metab* 2012; **32**: 425–436.
3 Arvanitakis Z, Leurgans SE, Barnes LL, Bennett DA, Schneider JA. Microinfarct pathology, dementia, and cognitive systems. *Stroke* 2011; **42**: 722–727.
4 Kövari E, Gold G, Herrmann FR, Canuto A, Hof PR, Bouras C *et al.* Cortical microinfarcts and demyelination affect cognition in cases at high risk for dementia. *Neurology* 2007; **68**: 927–931.
5 Van Veluw SJ, Zwanenburg JJ, Engelen-Lee J, Spliet WG, Hendrikse J, Luijten PR *et al. In vivo* detection of cerebral cortical microinfarcts with high-resolution 7T MRI. *J Cereb Blood Flow Metab* 2013; **33**: 322–329.
6 Van Veluw SJ, Jolink WM, Hendrikse J, Geerlings MI, Luijten PR, Biessels GJ *et al.* Cortical microinfarcts on 7T MRI in patients with spontaneous intracerebral hemorrhage. *J Cereb Blood Flow Metab* 2014; **34**: 1104–1106.
7 Van Veluw SJ, Heringa SM, Kuijf HJ, Koek HL, Luijten PR, Biessels GJ *et al.*. Cerebral cortical microinfarcts at 7Tesla MRI in patients with early Alzheimer's disease. *J Alzheimers Dis* 2014; **39**: 163–167.
8 Brundel M, Reijmer YD, van Veluw SJ, Kuijf HJ, Luijten PR, Kappelle LJ *et al.* Cerebral microvascular lesions on high-resolution 7T MRI in patients with type 2 diabetes. *Diabetes* 2014; **63**: 3523–3529.
9 Wardlaw JM, Smith EE, Biessels GJ, Cordonnier C, Fazekas F, Frayne R *et al.* Neuroimaging standards for research into small vessel disease and its contribution to ageing and neurodegeneration. *Lancet Neurol* 2013; **12**: 822–838.
10 Shoamanesh A, Kwok CS, Benavente O. Cerebral microbleeds: histopathological correlation of neuroimaging. *Cerebrovasc Dis* 2011; **32**: 528–534.
11 Fazekas F, Kleinert R, Roob G, Kleinert G, Kapeller P, Schmidt R *et al.* Histopathologic analysis of foci of signal loss on gradient-echo T2*-weighted MR images in patients with spontaneous intracerebral hemorrhage: evidence of microangiopathy-related microbleeds. *AJNR Am J Neuroradiol* 1999; **20**: 637–642.
12 Schrag M, McAuley G, Pomakian J, Jiffry A, Tung S, Mueller C *et al.* Correlation of hypointensities in susceptibility-weighted images to tissue histology in dementia patients with cerebral amyloid angiopathy: a postmortem MRI study. *Acta Neuropathol* 2010; **119**: 291–302.
13 De Reuck JL, Cordonnier C, Deramecourt V, Auger F, Durieux N, Bordet R *et al.* Microbleeds in postmortem brains of patients with Alzheimer disease: a T2*-weighted gradient-echo 7.0 T magnetic resonance imaging study. *Alzheimer Dis Assoc Disord* 2013; **27**: 162–167.
14 Ni J, Auriel E, Martinez-Ramirez S, Keil B, Reed AK, Fotiadis P *et al.* Cortical localization of microbleeds in cerebral amyloid angiopathy: an ultra high-field 7T MRI study. *J Alzheimers Dis* 2014; **43**: 1325–1330.
15 Greenberg SM, Vernooij MW, Cordonnier C, Viswanathan A, Al-Shahi Salman R, Warach S *et al.* Cerebral microbleeds: a guide to detection and interpretation. *Lancet Neurol* 2009; **8**: 165–174.
16 Kövari E, Herrmann FR, Hof PR, Bouras C. The relationship between cerebral amyloid angiopathy and cortical microinfarcts in brain ageing and Alzheimer's disease. *Neuropathol Appl Neurobiol* 2013; **39**: 498–509.
17 Soontornniyomkij V, Lynch MD, Mermash S, Pomekian J, Badkoobehi H, Clare R *et al.* Cerebral microinfarcts associated with severe cerebral beta-amyloid angiopathy. *Brain Pathol* 2010; **20**: 459–467.
18 Haglund M, Passant U, Sjöbeck M, Ghebremedhin E, Englund E. Cerebral amyloid angiopathy and cortical microinfarcts as putative substrates of vascular dementia. *Int J Geriatr Psychiatry* 2006; **21**: 681–687.
19 Shih AY, Blinder P, Tsai PS, Friedman B, Stanley G, Lyden PD *et al.* The smallest stroke: occlusion of one penetrating vessel leads to infarction and a cognitive deficit. *Nat Neurosci* 2013; **16**: 55–63.
20 Menon RS, Burgess RE, Wing JJ, Gibbons MC, Shara NM, Fernandez S *et al.* Predictors of highly prevalent brain ischemia in intracerebral hemorrhage. *Ann Neurol* 2012; **71**: 199–205.
21 Shoamanesh A, Catanese L, Sakai O, Pikula A, Kase CS. Diffusion-weighted imaging hyperintensities in intracerebral hemorrhage: microinfarcts or microbleeds? *Ann Neurol* 2013; **73**: 795–796.
22 Thomalla G, Cheng B, Ebinger M, Hao Q, Tourdias T, Wu O *et al.* DWI-FLAIR mismatch for the identification of patients with acute ischaemic stroke within 4.5 h of symptom onset (PRE-FLAIR): a multicentre observational study. *Lancet Neurol* 2011; **10**: 978–986.
23 Kim KW, MacFall JR, Payne ME. Classification of white matter lesions on magnetic resonance imaging in elderly persons. *Biol Psychiatry* 2008; **64**: 273–280.
24 Charidimou A, Jäger RH, Peeters A, Vandermeeren Y, Laloux P, Baron JC *et al.* White matter perivascular spaces are related to cortical superficial siderosis in cerebral amyloid angiopathy. *Stroke* 2014; **45**: 2930–2935.
25 Westover MB, Bianchi MT, Yang C, Schneider JA, Greenberg SM. Estimating cerebral microinfarct burden from autopsy samples. *Neurology* 2013; **80**: 1365–1369.
26 Ii Y, Maeda M, Kida H, Matsuo K, Shindo A, Taniguchi A *et al. In vivo* detection of cortical microinfarcts on ultrahigh-field MRI. *J Neuroimaging* 2013; **23**: 28–32.
27 Van Dalen JW, Scuric E, van Veluw SJ, Caan M, Nederveen AJ, Biessels GJ *et al.* Cortical microinfarcts detected *in vivo* on 3 Tesla MRI—clinical and radiological correlates. *Stroke* 2015; **46**: 255–257.
28 Van Veluw SJ, Hilal S, Kuijf HJ, Ikram MK, Xin X, Tan BY *et al.* Cortical microinfarcts on 3T MRI: clinical correlates in memory-clinic patients. *Alzheimers Dement* 2015 (in press).
29 Van Duijn S, Nabuurs RJ, van Rooden S, Maat-Schieman ML, van Duinen SG, van Buchem MA *et al.* MRI artifacts in human brain tissue after prolonged formalin storage. *Magn Reson Med* 2011; **65**: 1750–1758.

Supplementary Information accompanies the paper on the Journal of Cerebral Blood Flow & Metabolism website (http://www.nature.com/jcbfm)